Journal of Solid State Chemistry 182 (2009) 3269–3274

Contents lists available at ScienceDirect

Journal of Solid State Chemistry

journal homepage: www.elsevier.com/locate/jssc

New thallium iodates—Synthesis, characterization, and calculations of $Tl(IO_3)_3$ and $Tl_4(IO_3)_6$, $[Tl_3^+Tl^{3+}(IO_3)_6]$

Jeongho Yeon, Sang-Hwan Kim, P. Shiv Halasyamani *

Department of Chemistry, University of Houston, 136 Fleming Building, Houston, TX 77204-5003, USA

ARTICLE INFO

Article history:
Received 29 July 2009
Received in revised form
14 September 2009
Accepted 16 September 2009
Available online 23 September 2009

Keywords:
Thallium
Lone-pair
Crystal structures
Oxides
Iodates

ABSTRACT

Two new thallium iodates have been synthesized, $Tl(IO_3)_3$ and $Tl_4(IO_3)_6$ $[Tl_3^+Tl^{3+}(IO_3)_6]$, and characterized by single-crystal X-ray diffraction. Both materials were synthesized as phase-pure compounds through hydrothermal techniques using Tl_2CO_3 and HIO_3 as reagents. The materials crystallize in space groups *R*-3 ($Tl(IO_3)_3$) and *P*-1 ($Tl_4(IO_3)_6$). Although lone-pairs are observed for both I^{5+} and Tl^+, electronic structure calculations indicate the lone-pair on I^{5+} is stereo-active, whereas the lone-pair on Tl^+ is inert.

1. Introduction

Thallium, similar to other 6th period main-group metal cations such as lead and bismuth, is most commonly found in two oxidation states. For Tl these are +1 and +3, whereas for Pb and Bi the oxidation states are +2 and +4, and +3 and +5, respectively [1]. With the higher oxidation state symmetric coordination – usually octahedral – is observed, whereas with the lower oxidation state a lone-pair is formed. The lone-pair, which is also observed in other main-group metal cations such as Sn^{2+}, Sb^{3+}, and Te^{4+}, may either be inert or stereo-active [2–7]. With an inert lone-pair, the ns^2 electron pair remains highly localized and symmetric coordination environments around the cation are observed, whereas for a stereo-active lone-pair, bonding to the cation is highly asymmetric with the lone-pair on one-side of the coordination polyhedra 'pushing' the oxide ligands to the opposite side. With an inert lone-pair on Tl^+, the cation has a coordination environment similar to large alkali metals, e.g. Rb^+ and Cs^+ [6,7]. The occurrence of an inert or stereo-active lone-pair has profound implications for a variety of functional inorganic properties including second-order non-linear optical behavior and multiferroic behavior [8–13].

With respect to Tl^+ iodates, two compounds have been reported, $TlIO_3$ and $TlIO_4$ [14,15]. Both materials exhibit 'zero-dimensional' crystal structures containing Tl^+ cations separated by IO_3 or IO_4 anionic polyhedra. With respect to mixed-valent thallium compounds, i.e. those that contain Tl^+ and Tl^{3+}, a few compounds have been reported, for example $Tl_2(CrO_4)_2$ [16], Tl_4O_3 [17], $TlCl_{1.805}Br_{0.915}$ [18], Tl_2Cl_4 [19], $TlPd_3O_4$ [20], Tl_2Cl_3 [21], $Tl_3(OH)(SO_4)_2$ [22], $[Tl_3(Tl_{0.5}(H_3O)_{0.5})H_{14}(PO_4)](H_2O)_4$ [23], $Tl_{0.77}Sn_{0.61}Mo_7O_{11}$ [24], $Tl_2Nb_2O_7$ [25], $Tl(Tl_{0.6}Bi_{0.4})(CrO_4)_2$ [26], $Tl_2Os_2O_{6.77}$ [27], and Tl_2Br_3 [28]. Of these $Tl_2(CrO_4)_2$, $Tl_3(OH)(SO_4)_2$, and Tl_4O_3 are of particular relevance to our work, since the materials have a crystallographically unique Tl^+ and Tl^{3+} sites. In these three materials, the coordination for Tl^+ varies from three to eleven, whereas Tl^{3+} is in an octahedral coordination environment. The Tl^+, in $Tl_2(CrO_4)_2$ [16] and $Tl_3(OH)(SO_4)_2$ [22], is bonded to eight and nine, and eleven oxide ligands, respectively, creating a symmetric coordination environment, that suggests the lone-pair is inert, whereas the Tl^+ in Tl_4O_3 [17] is linked to three, four, and five oxide ligands, in highly asymmetric coordination environments indicating the lone-pair is more stereo-active. In this paper, we report on the synthesis, structure, characterization and electronic structure calculations of two new thallium iodates, $Tl(IO_3)_3$ and $Tl_4(IO_3)_6$ $[Tl_3^+Tl^{3+}(IO_3)_6]$. The latter represents a rare example of a mixed-valent and crystallographically ordered Tl^+/Tl^{3+} compound (Tables 1–4).

2. Experimental section

2.1. Reagents

Tl_2CO_3 (Alfa Aesar, 99.9+%) and HIO_3 (Alfa Aesar, 99.5%) were used as received.

* Corresponding author. Fax: +1 713 743 0796.
E-mail address: psh@uh.edu (P.S. Halasyamani).

0022-4596/$ - see front matter © 2009 Elsevier Inc. All rights reserved.
doi:10.1016/j.jssc.2009.09.021

Table 1
Crystallographic data for $Tl(IO_3)_3$ and $Tl_4(IO_3)_6$.

Formula	$Tl(IO_3)_3$	$Tl_4(IO_3)_6$
fw	729.07	933.44
Cryst dimensions (mm^3)	$0.06 \times 0.09 \times 0.09$	$0.04 \times 0.05 \times 0.05$
Color	Colorless	Pale yellow
Crystal system	Trigonal	Triclinic
Space group	*R*-3 (No. 148)	*P*-1 (No. 2)
a (Å)	9.8459(6)	7.1087(5)
b (Å)	9.8459(6)	7.1168(5)
c (Å)	14.2492(18)	10.6176(8)
α (°)	90	87.4460(10)
β (°)	90	72.3760(10)
γ (°)	120	72.3880(10)
V ($Å^3$)	1196.28(18)	487.29(6)
Z	6	2
T (°C)	23	23
λ (Å)	0.71073	0.71073
ρ_{calcd} ($g\,cm^{-3}$)	6.072	6.362
μ (mm^{-1})	31.890	42.554
2θ max (deg.)	59.80	59.44
No. of reflections collected/unique	2496/659	3096/2241
Abs corr.	Ψ-scan	Ψ-scan
R (int)	0.0325	0.0349
GOF	1.181	1.074
Extinction coefficient	0.00032(3)	0.0033(2)
$R(F)$[a]	0.0159	0.0294
$R_w(F_o^2)$[b]	0.0375	0.0773

[a] $R(F)=\sum||F_o|-|F_c||/\sum|F_o|$.
[b] $R_w(F_o^2)=[\sum w(F_o^2-F_c^2)^2/\sum w(F_o^2)^2]^{1/2}$.

Table 2
Atomic coordinates and equivalent isotropic displacement parameters ($Å^2 \times 10^3$) for $Tl(IO_3)_3$.

Atoms	*x*	*y*	*z*	U_{eq}[a]
Tl(1)	2/3	1/3	0.1574(1)	12(1)
I(1)	0.0352(1)	0.6636(1)	0.2490(1)	14(1)
O(1)	0.8241(4)	0.5388(4)	0.2441(2)	18(1)
O(2)	0.0334(4)	0.8444(4)	0.2769(2)	15(1)
O(3)	0.0846(5)	0.6983(4)	0.1263(3)	27(1)

[a] U_{eq} is defined as one-third of the trace of the orthogonalized U_{ij} tensor.

Table 3
Atomic coordinates and equivalent isotropic displacement parameters ($Å^2 \times 10^3$) for $Tl_4(IO_3)_6$.

Atoms	*x*	*y*	*z*	U_{eq}[a]
Tl(1)	1/2	0	0	10(1)
Tl(2)	0.1626(1)	−0.4658(1)	−0.4016(1)	24(1)
Tl(3)	0	1/2	0	26(1)
I(1)	0.5526(1)	−0.4612(1)	−0.1915(1)	10(1)
I(2)	0.0310(1)	0.0262(1)	−0.1893(1)	10(1)
I(3)	0.5848(1)	0.0561(1)	−0.3674(1)	10(1)
O(1)	0.4661(9)	0.1208(9)	−0.1882(5)	18(1)
O(2)	−0.1620(9)	−0.0451(9)	−0.0483(6)	20(1)
O(3)	0.5653(10)	−0.3266(8)	−0.0520(5)	18(1)
O(4)	0.6774(10)	−0.3358(9)	−0.3255(6)	21(1)
O(5)	0.2857(9)	−0.3500(9)	−0.1867(6)	20(1)
O(6)	−0.0462(10)	−0.0457(10)	−0.3209(6)	25(1)
O(7)	−0.0818(10)	0.2913(8)	−0.1815(6)	22(1)
O(8)	0.5862(10)	0.3056(9)	−0.4099(6)	20(1)
O(9)	0.3388(9)	0.0631(9)	−0.3897(5)	18(1)

[a] U_{eq} is defined as one-third of the trace of the orthogonalized U_{ij} tensor.

2.2. Synthesis

For $Tl(IO_3)_3$, 0.125 g (2.66×10^{-4} mol) of Tl_2CO_3 and 1.88 g (1.07×10^{-2} mol) of HIO_3 were combined with 9 ml deionized H_2O. For $Tl_4(IO_3)_6$, 0.727 g (1.55×10^{-3} mol) of Tl_2CO_3 and 1.27 g (7.24×10^{-3} mol) of HIO_3 were combined with 9 ml of deionized H_2O. The reactants were placed in separate 23-ml Teflon-lined autoclaves that were subsequently sealed. The autoclaves were gradually heated to 230 °C, held for 4 days, and cooled slowly to room temperature at 6 °C h^{-1}. The mother liquor was decanted from the products, and the products were recovered by filtration and washed with water and acetone. Clear colorless or pale yellow crystals, the only product from each reaction, of $Tl(IO_3)_3$ and $Tl_4(IO_3)_6$ were obtained in approximately 70% and 90% yields, respectively, based on Tl_2CO_3. It is suggested that during the $Tl_4(IO_3)_6$ reaction the I^{5+} in HIO_3 is reduced to I_2 concomitant with the oxidation of Tl^+ to Tl^{3+}. In fact, after the reaction, blue-black blocks were observed in the products that were subsequently shown to be I_2 by the starch test [29]. The I_2 was easily removed through washing with acetone.

Table 4
Selected bond distances (Å) for $Tl(IO_3)_3$ and $Tl_4(IO_3)_6$.

$Tl(IO_3)_3$		$Tl_4(IO_3)_6$	
Tl(1)–O(1) × 3	2.210(3)	Tl(1)–O(1) × 2	2.191(5)
Tl(1)–O(2) × 3	2.243(3)	Tl(1)–O(2) × 2	2.223(6)
		Tl(1)–O(3) × 2	2.287(5)
I(1)–O(1)	1.811(3)		
I(1)–O(2)	1.833(3)	Tl(2)–O(4)	3.014(6)
I(1)–O(3)	1.802(4)	Tl(2)–O(4)	3.139(6)
		Tl(2)–O(5)	2.909(6)
		Tl(2)–O(6)	2.941(7)
		Tl(2)–O(7)	3.234(6)
		Tl(2)–O(8)	2.713(6)
		Tl(2)–O(8)	2.934(7)
		Tl(2)–O(9)	3.216(6)
		Tl(3)–O(2) × 2	3.166(6)
		Tl(3)–O(3) × 2	3.169(6)
		Tl(3)–O(5) × 2	2.807(6)
		Tl(3)–O(7) × 2	2.778(6)
		I(1)–O(4)	1.791(6)
		I(1)–O(5)	1.807(6)
		I(1)–O(3)	1.838(5)
		I(2)–O(2)	1.868(6)
		I(2)–O(6)	1.793(6)
		I(2)–O(7)	1.808(6)
		I(3)–O(1)	1.848(5)
		I(3)–O(8)	1.815(6)
		I(3)–O(9)	1.820(6)

2.3. Single-crystal X-ray diffraction

For $Tl(IO_3)_3$, a colorless multi-faceted crystal ($0.06 \times 0.09 \times 0.09\,mm^3$) and for $Tl_4(IO_3)_6$, a pale yellow block-shaped crystal ($0.04 \times 0.05 \times 0.05\,mm^3$) were used for single-crystal data analyses. Data were collected using a Siemens SMART diffractometer equipped with a 1K CCD area detector using graphite-monochromated Mo $K\alpha$ radiation. A hemisphere of data was collected using a narrow-frame method with scan widths of 0.30° in omega and an exposure time of 35 s per frame. The first 50 frames were remeasured at the end of the data collection to monitor instrument and crystal stability. The maximum correction applied to the intensities was $<1\%$. The data were integrated using the Siemens SAINT program [30], with the intensities corrected for Lorentz, polarization, air absorption, and absorption attributable to the variation in the path length through the detector faceplate. Ψ-Scans were used for the absorption correction on the hemisphere of data. The data were solved by direct methods using SHELXS-97 and refined using SHELXL-97 [31,32]. All of the atoms were refined with anisotropic thermal parameters and converged

for $I > 2\sigma(I)$. All calculations were performed using the WinGX-98 crystallographic software package [33].

2.4. Powder X-ray diffraction

Powder X-ray diffraction was used to confirm the phase purity of the sample. The X-ray powder diffraction data were collected on a PANalytical X'PertPRO diffractometer at room temperature (Cu $K\alpha$ radiation, flat plate geometry) equipped with X'Celerator detector in the 2θ range 5–60° with a step size of 0.02° and a step time of 0.8 s.

2.5. Infrared (IR) spectroscopy

Infrared spectra were recorded on a Matteson FT-IR 5000 spectrometer in the 400–4000 cm^{-1} range, with the sample pressed between two KBr pellets.

2.6. UV–vis diffuse reflectance spectroscopy

UV–vis diffuse reflectance data were collected on a Varian Cary 500 scan UV–vis–NIR spectrophotometer over the spectral range 200–1500 nm at room temperature. Poly-(tetrafluoroethylene) was used as a reference material. Reflectance spectra were converted to absorbance with the Kubelka–Munk function [34,35].

2.7. Calculations

First principle density functional electronic band structures for $Tl(IO_3)_3$ and $Tl_4(IO_3)_6$ were carried out using plane wave pseudopotential calculations as implemented in the Quantum ESPRESSO (4.0.1 version) package [36]. Norm-conserving Martins–Troullier (MT) pseudopotentials [37] were utilized with the generalized gradient approximation (GGA) [38] for the exchange-correlation corrections. The pseudopotentials generated from Fritz-Haber-Institute (FHI) code were converted for the calculations. A plane wave energy cutoff was set to 37 Ry. For Brillouin zone integration, k-point grids of $6 \times 6 \times 4$ and $4 \times 4 \times 4$ were utilized for $Tl(IO_3)_3$ and $Tl_4(IO_3)_3$, respectively, where the primitive rhombohedral unit cell of $Tl(IO_3)_3$ was chosen for the calculations. A total energy convergence threshold was set to 10^{-6} Ry.

2.8. Thermogravimetric analysis (TGA)

Thermogravimetric analyses were carried out on a TGA 951 thermogravimetric analyzer (TA instruments). The sample was placed within a platinum crucible and heated in N_2 gas at a rate of 10 °C min^{-1} to 900 °C.

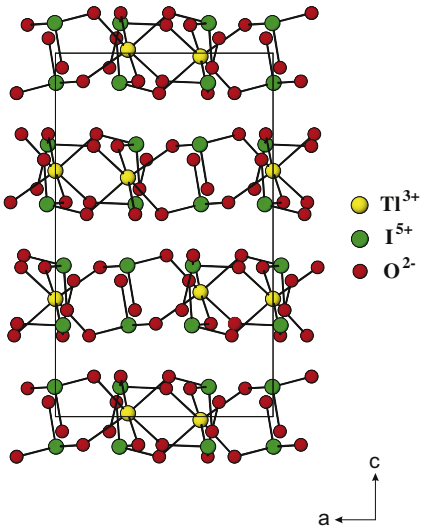

Fig. 1. Ball-and-stick representation of $Tl(IO_3)_3$ in the *ac*-plane. The stereo-active lone-pair on I^{5+} is directed toward the gaps between the layers.

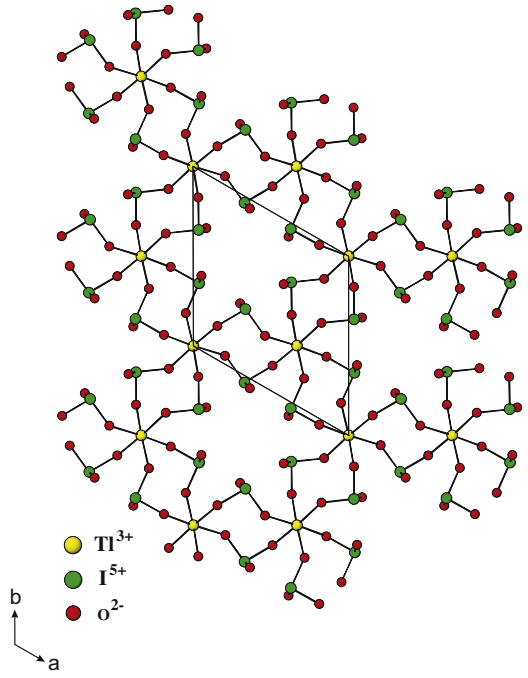

Fig. 2. Ball-and-stick representation of layer of $Tl(IO_3)_3$. All six oxide ligands linked to Tl^{3+} are also bonded to I^{5+} cations.

3. Results and discussion

3.1. Structures

$Tl(IO_3)_3$ and $Tl_4(IO_3)_6$ exhibit two- and 'zero-dimensional' crystal structures, respectively. $Tl(IO_3)_3$, which is structurally similar to $In(IO_3)_3$ [39–41], has a layered crystal structure, consisting of TlO_6 octahedra that are linked to six IO_3 polyhedra through oxide bonds (see Fig. 1). A ball-and-stick representation of the layer is shown in Fig. 2. The major difference between $Tl(IO_3)_3$ and $In(IO_3)_3$ is the M^{3+}-oxygen bond lengths. For $Tl(IO_3)_3$, the Tl–O bonds range in distance from 2.210(3) to 2.243(3) Å, whereas in $In(IO_3)_3$ the corresponding In–O bonds are shorter, ranging between 2.141(3) and 2.156(3)Å [39–41]. In $Tl(IO_3)_3$, the stereo-active lone-pair on I^{5+} point in the 'gaps' between the layers. In connectivity terms, the compound may be written as $\{[TlO_{6/2}]^{3-}\ 3[IO_{2/2}O_{1/1}]^{+}\}^{0}$. $Tl_4(IO_3)_6$, which may also be written as $[Tl_3^{+}Tl^{3+}(IO_3)_6]$, exhibits a 'zero-dimensional' crystal structure. As seen in Fig. 3, a $Tl^{3+}O_6$ octahedron is connected to six IO_3 polyhedra through oxide bonds. These polyhedral groups are separated by Tl^{+} cations. In connectivity terms, the compound may be written as $\{[TlO_{6/2}]^{3-}\ 6[IO_{1/2}O_{2/1}]^{0}\}^{3-}$, with charge balance maintained by three Tl^{+} cations. In $Tl(IO_3)_3$ and $Tl_4(IO_3)_6$, the Tl^{3+} cation is octahedrally coordinated to six oxygen atoms, with bond distances ranging from 2.191(5) to 2.287(5)Å. The two unique Tl^{+} cations in $Tl_4(IO_3)_6$ are in eight-fold

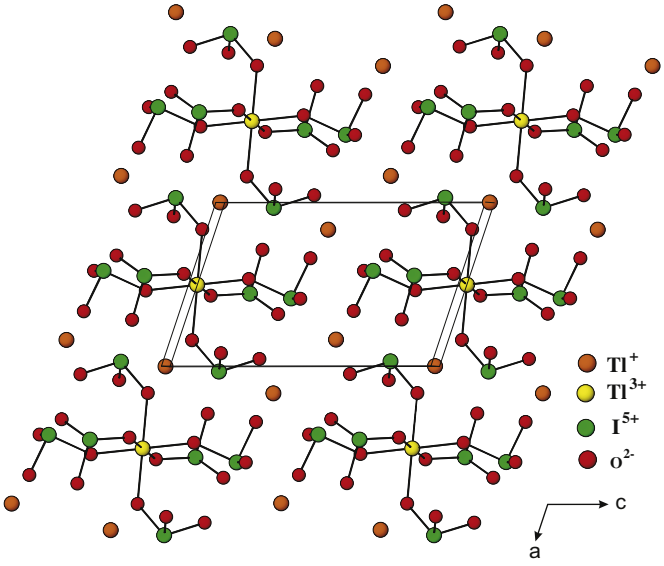

Fig. 3. Ball-and-stick representation of 'zero-dimensional' $Tl_4(IO_3)_6$ in the *ac*-plane. The $[Tl(IO_3)_6]^{3-}$ anions are separated by the Tl^+ cations.

coordination environments with bond distances ranging from 2.713(6) to 3.234(6)Å. As we will demonstrate, the lone-pair on Tl^+ may be considered as inert rather than stereo-active, resulting in a coordination environment similar to large alkali metal cations [6,7]. Finally, in both materials the I^{5+} cation is in a trigonal pyramidal coordination environment, attributable to its stereo-active lone-pair, with I–O distances ranging from 1.791(6) to 1.868(6)Å. Bond valence calculations [42,43] revealed values of 0.96 and 1.11 for Tl^+ in $Tl_4(IO_3)_6$, 3.24 and 3.30 for Tl^{3+}, and 4.82–5.03 for I^{5+} in both compounds.

3.2. IR spectroscopy

The IR spectra of $Tl_4(IO_3)_6$ and $Tl(IO_3)_3$ iodates indicated Tl–O vibrations in the region of ca. 800 cm^{-1} and I–O vibrations in the region of ca. 650–760 and 400–500 cm^{-1}. These vibrations are consistent with those previously reported [44–49]. The IR vibrations and assignments have been deposited in the Supporting Information.

3.3. UV–vis diffuse reflectance spectroscopy

$Tl(IO_3)_3$ is white, whereas $Tl_4(IO_3)_6$ is pale yellow. The UV–vis spectra revealed that the reported iodates are transparent to approximately 2.8–3.5 eV. Absorption (*K*/*S*) data were calculated by using the Kubelka–Munk function [34,35]:

$$F(R) = \frac{(1-R)^2}{2R} = \frac{K}{S}$$

with *R* representing the reflectance, *K* the absorption, and *S* the scattering. In a *K*/*S* versus *E* (eV) plot, extrapolating the linear part of the rising curve to zero provides the onset of absorption at 3.4 eV for $Tl(IO_3)_3$ and 2.9 eV for $Tl_4(IO_3)_6$. This observation is qualitatively consistent with the values from electronic structure calculations. Briefly, in both materials a narrow conduction band above the Fermi level, E_F, is observed and has equal contributions from the Tl-6*s*, I-5*p* and O-2*sp* orbitals. Below E_F, in $Tl(IO_3)_3$ we observe mainly O-2*sp* orbital contributions with a minor amount of I-5*s* orbital contributions, and a negligible contribution from Tl-6*sp*, whereas in $Tl_4(IO_3)_6$ at equivalent energies we observe similar O-2*sp* and I-5*sp* orbital contributions, but also contributions from Tl-6*s* (Tl^+ cation) orbitals. Thus the optical band gap in $Tl(IO_3)_3$ and $Tl_4(IO_3)_6$ may be attributed to ligand-to-metal, oxygen to thallium or iodine, charge transfer, with additional complexity from the Tl^+ cation in $Tl_4(IO_3)_6$. The UV–vis diffuse reflectance spectra for the reported compounds have been deposited in the Supporting Information.

3.4. Calculations

The electronic band structures of $Tl(IO_3)_3$ and $Tl_4(IO_3)_6$ were performed using pseudopotential calculations. Fig. 4 reveals the total and projected density of states (TDOSs) and (PDOSs), respectively, for $Tl(IO_3)_3$ and $Tl_4(IO_3)_6$. Both electronic structures show an energy gap appearing at the Fermi level (E_F) as indicative of a band gap. The calculated gaps are approximately 2.2 and 1.8 eV for $Tl(IO_3)_3$ and $Tl_4(IO_3)_6$, respectively, and are smaller by 1.2 and 1.1 eV than the experimentally observed energy gap in

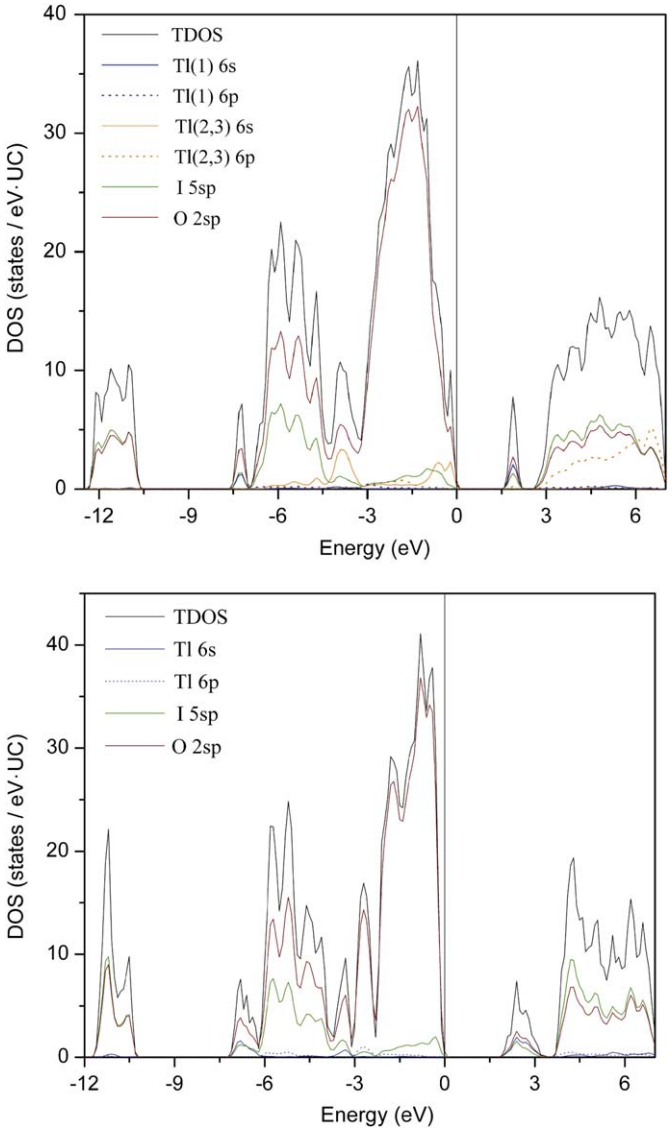

Fig. 4. The TDOS and PDOSs of the $Tl(IO_3)_3$ (top) and $Tl_4(IO_3)_6$ (bottom) using pseudopotential calculations. The vertical line at 0 eV indicates the Fermi level, EF. TDOS: black solid line; PDOS: blue and orange solid line—Tl-6*s*; blue and orange dotted line—Tl-6*p*; green solid line—I-5*sp*; brown solid line—O2*sp*. For interpretation of the references to color in this figure legend, the reader is referred to the web version of this article.

their UV–vis diffuse reflectance spectra. This discrepancy could be explained by the underestimation of the band gap that results in an overestimation of band width [50–52]. The electronic structure of $Tl(IO_3)_3$ reveals a narrow valence band at ~ -11 eV, and a complex broad band from ~ -7 eV to E_F. From the detailed PDOS analyses, we deduce that the narrow band is mainly composed of I-5*s* and O-2*s* orbitals. The lower part of the broad band (-7 to -4 eV) consists of mainly O-2*p* and I-5*p* orbitals, whereas the upper part (-4 eV to E_F) is mainly composed of O-2*sp* orbitals. Likewise, similar patterns of the I-5*sp* and O-2*sp* orbital contributions are found for the narrow and broad valence bands for $Tl_4(IO_3)_6$ except for the Tl-6*sp* orbital contribution. From the Tl-6*s* and -6*p* PDOSs orbital analyses, the Tl-6*sp* contribution in $Tl(IO_3)_3$ is negligible below E_F, consistent with the assigned oxidation state and bond valence sum of +3 for Tl. Similarly, in $Tl_4(IO_3)_6$, the contribution of Tl(1)-6*sp* (Tl^{3+}) is negligible, whereas the contributions of Tl(2)-6*s* and Tl(3)-6*s*, both Tl^+ cations – hereafter called Tl(2,3)-6*s* – are shown below E_F (see Fig. 4). These calculations are in good agreement with the Tl(1) and Tl(2,3) assigned oxidation states and bond valence sums of +3 and +1, respectively. Overall, the I-5*p* orbital contributes significantly below the Fermi level, whereas the Tl-6*p* orbital contribution is negligible. The lone-pair of Tl^+ is expected to be highly symmetric and inert attributable to the absence of the Tl-6*p* orbital mixing into the Tl–O interaction [53–55]. Thus, stereo-active lone-pair formation is anticipated only near the I^{5+} but not the Tl^+ [5–7]. To examine the character of the lone-pairs on I^{5+} and Tl^+, electron localization function (ELF) calculations [56,57] were performed for $Tl(IO_3)_3$ and $Tl_4(IO_3)_6$ using the pseudo-potential method. The ELF visualization of the compounds with η=0.9 are shown in Fig. 5 where a lobe-like iso-surface is clearly observed near the I^{5+} in both compounds [6,7,46]. The iso-surface may be considered as the stereo-active lone-pair, whereas a sphere-like iso-surface exhibited at Tl(2) and Tl(3) sites in $Tl_4(IO_3)_6$ can be considered as an inert pair [6,7], attributable to the absence of the Tl-6*p* mixing into the weak Tl(6*s*)–O(2*p*) interaction below the Fermi level.

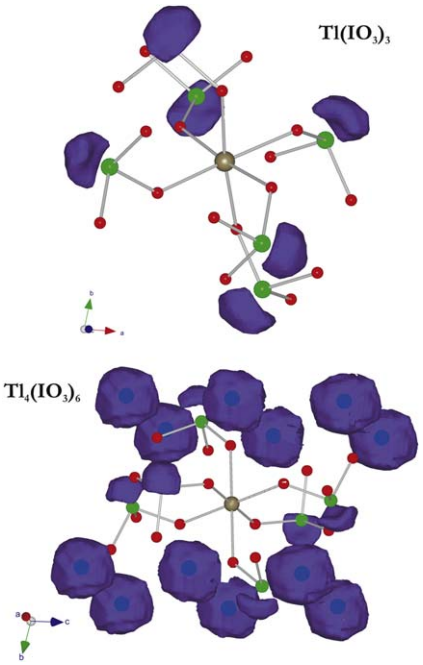

Fig. 5. Visualization of the stereo-active lone-pair (purple) through electron localization function (ELF) for the $Tl(IO_3)_3$ (top) and $Tl_4(IO_3)_6$ (bottom) with η=0.9 from the pseudopotential calculations. The dark blue spheres in $Tl_4(IO_3)_6$ are the Tl^+ cations. For interpretation of the references to color in this figure legend, the reader is referred to the web version of this article.

3.5. Thermal analyses

The thermal behavior of the reported iodate compounds was investigated using thermogravimetric analysis (TGA). $Tl(IO_3)_3$ and $Tl_4(IO_3)_6$ are not stable at higher temperatures, as both iodate compounds have three decomposition steps before volatilization. For $Tl(IO_3)_3$, two equivalents of I_2 and three equivalents of O_2 are lost at approximately 480 °C. Calc. (exp.): 47.98% (48.02%). In the second step, one equivalent I_2 and 1.5 equivalents O_2 are lost at around 560 °C resulting in 1 mol of Tl_2O_3, calc. (exp.): 68.68% (70.86%). The remaining Tl_2O_3 begins to volatilize around 590 °C. For $Tl_4(IO_3)_6$, one equivalent of I_2 and three equivalents of O_2 are lost at approximately 480 °C, calc. (exp.): 18.74% (18.63%). Above 480 °C, two equivalents I_2 and three equivalents O_2 are lost leaving 2 mol of Tl_2O_3 at around 560 °C, calc. (exp.): 51.07% (54.56%). Finally, the remaining Tl_2O_3 starts to volatilize around 590 °C. The XRD powder patterns were measured to check the residue in each decomposition step. It was confirmed that the decomposition before volatilization resulted in Tl_2O_3 through the decomposition of $TlIO_3$. The TGA curves and the XRD powder patterns for each decomposition step with both materials have been deposited in the Supporting Information.

4. Conclusion

Two new thallium iodates, $Tl(IO_3)_3$ and $Tl_4(IO_3)_6$, have been synthesized through hydrothermal techniques. Interestingly, $Tl_4(IO_3)_6$ represents a rare example of a mixed-valent and crystallographically ordered Tl^+/Tl^{3+} compound. Layered and 'zero-dimensional' crystal structures are observed for $Tl(IO_3)_3$ and $Tl_4(IO_3)_6$, respectively. Electronic structure calculations indicate that both I^{5+} and Tl^+ exhibit a lone-pair. The lone-pair, however, is stereo-active for I^{5+} and inert on Tl^+, resulting in asymmetric and symmetric coordination environments, respectively. We are in the process of synthesizing other Tl^+ compounds and will be reporting on them shortly.

Acknowledgments

We thank the Robert A. Welch Foundation (Grant E-1457), the ACS PRF 47345-AC10, and the NSF (DMR-0652150) for support.

Appendix A. Supplementary material

Supplementary data associated with this article can be found in the online version at doi:10.1016/j.jssc.2009.09.021.

References

[1] N.N. Greenwood, A. Earnshaw (Eds.), Chemistry of the Elements, Butterworth-Heinemann, Oxford, 1999.
[2] J. Galy, G. Meunier, S. Andersson, A. Astrom, J. Solid State Chem. 13 (1975) 142–159.
[3] A. -V. Mudring, F. Rieger, Inorg. Chem. 44 (2005) 6240–6243.
[4] F. Rieger, A. -V. Mudring, Inorg. Chem. 46 (2007) 446–452.
[5] M.W. Stoltzfus, P. Woodward, R. Seshadri, J. -H. Park, B. Bursten, Inorg. Chem. 46 (2007) 3839–3850.
[6] H.Y. Chang, S. -H. Kim, K.M. Ok, P.S. Halasyamani, Chem. Mater. 21 (2009) 1654–1662.
[7] H.Y. Chang, S. -H. Kim, K.M. Ok, P.S. Halasyamani, J. Am. Chem. Soc. 131 (2009) 6865–6873.

[8] J.G. Bergman, G.D. Boyd, A. Ashkin, S.K. Kurtz, J. Appl. Phys. 40 (1969) 2860–2863.
[9] J.G. Bergman, G.R. Crane, J. Solid State Chem. 12 (1975) 172–175.
[10] R. Seshadri, N.A. Hill, Chem. Mater. 13 (2001) 2892–2899.
[11] P.S. Halasyamani, Chem. Mater. 16 (2004) 3586–3592.
[12] P. Baettig, C. Ederer, N.A. Spaldin, Phys. Rev. B: Condens. Matter Mater. Phys. 72 (2005) 214105/1–214105/8.
[13] C. Ederer, C.J. Fennie, J. Phys.: Condens. Matter 20 (2008) 434219/1–434219/8.
[14] J.G. Bergman, J.S. Wood, Acta Crystallogr. Sect. C 43 (1987) 1831–1832.
[15] F.M. Jaeger, J. Beintema, Proc. K. Ned. Akad. Wet. 36 (1933) 523–528.
[16] P.A. Koz'min, M.D. Surazhskaya, Zh. Strukt. Khim. 9 (1968) 917.
[17] R. Marchand, M. Tournoux, C. R. Acad. Sci. Ser. C 277 (1973) 863–865.
[18] G. Thiele, W. Rink, Z. Anorg. Allg. Chem. 414 (1975) 47–55.
[19] G. Thiele, W. Rink, Z. Anorg. Allg. Chem. 414 (1975) 231–235.
[20] C. Zoellner, G. Thiele, M. Muellner, Z. Anorg. Allg. Chem. 443 (1978) 11–18.
[21] R. Boehme, J. Rath, B. Grunwald, G. Thiele, Z. Naturforsch, B: Anorg. Chem. Org. Chem. 35 (1980) 1366–1372.
[22] F. Abraham, G. Nowogrocki, B. Jolibois, G. Laplace, J. Solid State Chem. 47 (1983) 1–5.
[23] R.E. Marsh, Acta Crystallogr. C 42 (1986) 511–512.
[24] R. Dronskowski, A. Simon, Acta Chem. Scand. 45 (1991) 850–855.
[25] J.L. Fourquet, H. Duroy, P. Lacorre, J. Solid State Chem. 114 (1995) 575–584.
[26] Y.G. Cudennec, A. Riou, A. Lecerf, C.R. Acad. Sci. Paris T. 1 Serie II 1 (1998) 247–252.
[27] J. Reading, C.S. Knee, M.T. Weller, J. Mater. Chem. 12 (2002) 2376–2382.
[28] R. Ackermann, C. Hirschle, H.W. Rotter, G.Z. Thiele, Z. Anorg. Allg. Chem. 628 (2002) 2675–2682.
[29] N.N. Greenwood, A. Earnshaw (Eds.), Chemistry of the Elements, Butterworth-Heinemann, Oxford, 1999, p. 864.
[30] SAINT, Program for Area Detector Absorption Correction, version 4.05, Siemens Analytical X-ray Instruments, Madison, WI, 1995.
[31] G.M. Sheldrick, SHELXL-97, A program for crystal structure refinement, University of Gottingen, Gottingen, Germany, 1997.
[32] G.M. Sheldrick, SHELXS-97, A program for automatic solution of crystal structures, University of Gottingen, Gottingen, Germany, 1997.
[33] L.F. Farrugia, J. Appl. Crystallogr. 32 (1999) 837–838.
[34] P. Kubelka, F.Z. Munk, Tech. Phys. 12 (1931) 593.
[35] J. Tauc, Mater. Res. Bull. 5 (1970) 721–729.
[36] S. Baroni, A. Dal Corso, S. de Gironcoli, P. Giannozzi, C. Cavazzoni, G. Ballabio, S. Scandolo, G. Chiarotti, P. Focher, A. Pasquarello, K. Laasonen, A. Trave, R. Car, N. Marzari, A. Kokalj, Quantum-ESPRESSO version 4.0.1, 〈http://www.quantum-espresso.org/〉.
[37] N. Troullier, J.L. Martins, Phys. Rev. B 43 (1991) 1993–2006.
[38] J.P. Perdew, K. Burke, M. Ernzerhof, Phys. Rev. Lett. 77 (1996) 3865–3868.
[39] O.A. Gurbanova, A.C. Ivanova, E.L. Belokoneva, O.V. Dimitrova, N.N. Mochenova, Crystallogr. Rep. 53 (1) (2008) 47–52.
[40] D. Phanon, A. Mosset, I. Gautier-Luneau, J. Mater. Chem. 17 (11) (2007) 1123–1130.
[41] N. Ngo, K. Kalachnikova, Z. Assefa, R.G. Haire, R.E. Sykora, J. Solid State Chem. 179 (12) (2006) 3824–3830.
[42] I.D. Brown, D. Altermatt, Acta Crystallogr. Sect. B 41 (1985) 244–247.
[43] N.E. Brese, M. O'Keeffe, Acta Crystallogr. Sect. B 47 (1991) 192–197.
[44] S.R. Sagi, M.S.P. Rao, K.V. Ramana, J. Therm. Anal. 20 (1981) 93–100.
[45] E.F. Archibong, R. Sullivan, J. Phys. Chem. 100 (1996) 18078–18082.
[46] H.-Y. Chang, S.-H. Kim, P.S. Halasyamani, K.M. Ok, J. Am. Chem. Soc. 131 (2009) 2426–2427.
[47] K.M. Ok, P.S. Halasyamani, Inorg. Chem. 44 (2005) 9353–9359.
[48] R.E. Sykora, K.M. Ok, P.S. Halasyamani, T.E. Albrecht-Schmitt, J. Am. Chem. Soc. 124 (2002) 1951–1957.
[49] R.E. Sykora, K.M. Ok, P.S. Halasyamani, D.M. Wells, T.E. Albrecht-Schmitt, Chem. Mater. 14 (2002) 2741–2749.
[50] H. Mizoguchi, H.W. Eng, P.M. Woodward, Inorg. Chem. 43 (2004) 1667–1680.
[51] H. Mizoguchi, P.M. Woodward, Chem. Mater. 16 (2004) 5233–5248.
[52] H.W. Eng, P.W. Barnes, B.M. Auer, P.M. Woodward, J. Solid State Chem. 175 (2003) 94–109.
[53] I. Lefebvre, M.A. Szymanski, J. Olivier-Fourcade, J.C. Jumas, Phys. Rev. B 58 (1998) 1896–1906.
[54] G.W. Watson, S.C. Parker, G. Kresse, Phys. Rev. B 59 (1999) 8481–8486.
[55] G.W. Watson, S.C. Parker, J. Phys. Chem. B 103 (1999) 1258–1262.
[56] A.D. Becke, K.E. Edgecombe, J. Chem. Phys. 92 (1990) 5397–5403.
[57] A. Savin, O. Jepsen, J. Flad, O.K. Andersen, H. Preuss, H.G. Von Schnering, Angew. Chem. Int. Ed. 31 (1992) 187–188.